Thermal dynamics on the lattice with exponentially improved accuracy

J. M. Pawlowski [1,2] and A. Rothkopf [1]

[1] *Institute for Theoretical Physics, Universität Heidelberg, Philosophenweg 12, D-69120 Germany*
[2] *ExtreMe Matter Institute EMMI, GSI, Planckstr. 1, D-64291 Darmstadt, Germany*

We present a novel simulation prescription for thermal quantum fields on a lattice that operates directly in imaginary frequency space. By distinguishing initial conditions from quantum dynamics it provides access to correlation functions also outside of the conventional Matsubara frequencies $\omega_n = 2\pi n T$. In particular it resolves their frequency dependence between $\omega = 0$ and $\omega_1 = 2\pi T$, where the thermal physics $\omega \sim T$ of e.g. transport phenomena is dominantly encoded. Real-time spectral functions are related to these correlators via an integral transform with rational kernel, so their unfolding is exponentially improved compared to Euclidean simulations.

We demonstrate this improvement within a $0+1$-dimensional scalar field theory and show that spectral features inaccessible in standard Euclidean simulations are quantitatively captured.

arXiv:1610.09531v1 [hep-lat] 29 Oct 2016

Modern experiments ranging from heavy-ion collisions at RHIC and LHC [1, 2] to ultracold quantum gases [3] explore the physics of strongly-correlated quantum systems across vastly separated temperature scales ($T \sim 10^{12}..10^{-9}K$) [4]. A unifying aspect of these studies are thermal phenomena, such as the transport of conserved charges [5–16] or the in-medium modification of heavy bound states [17–23]. Connecting these to fundamental interactions, such as QED and QCD, requires a thorough theoretical understanding of the equilibrium properties of quantum fields. Unfortunately in realistic experimental environments many approximate techniques, such as perturbation theory, are inapplicable and a non-perturbative numerical computation is required.

Conventional simulations of quantum fields, e.g. lattice QCD, are based on non-perturbative Monte-Carlo techniques relying on an analytic continuation of the real-time axis into the complex plane [24, 25], for real-time approaches to spectral functions see e.g. [8–10, 26–33].

Two conceptual challenges plague the necessary reconstruction of real-time correlation functions from those simulated in imaginary time: the crucial one is the finite extent of the Euclidean time axis with $\tau \in [0\,,\,1/T]$. It leads to discrete Matsubara frequencies $\omega_n = 2\pi n T$, which limits the resolution of imaginary frequencies. In turn, increasing the number of temporal points N_τ simply increases the maximum frequency available while keeping the spacing fixed. Thus, a large N_τ does not improve the access to the relevant regime $\omega \sim T$, where thermal physics is dominantly encoded in $G(\omega)$. The signal to noise ratio for thermal contributions actually decays rapidly above $\omega \approx T$ and indeed, already $G(\omega_1 = 2\pi T)$ may only be marginally relevant for thermal physics.

In order to resolve this conceptual issue, we present a simulation algorithm, which operates in imaginary frequency space with arbitrary resolution, given by the number of frequency points N_ω. In particular this approach resolves frequencies between ω_0 and ω_1.

The second issue concerns the unfolding of spectral functions $\rho(\mu)$ from imaginary time correlators $G(\tau)$, or imaginary frequency correlators $G(\omega)$. In Euclidean time the inverse problem reads

$$G(\tau) = \int d\mu\, \tilde{K}(\mu,\tau,T)\rho(\mu), \quad \tilde{K}(\mu,\tau,T) \overset{\mu\tau\gg 1}{\sim} e^{-\mu\tau}\,. \tag{1}$$

Eq. (1) leads to an exponentially hard ill-posed problem [34]. In this work we simulate directly in imaginary frequency space, where numerical data and spectral functions are related via the rational Källén-Lehmann kernel,

$$G(\omega) = \int d\mu\, K(\mu,\omega)\rho(\mu), \quad |K(\mu,\omega)| \overset{\mu/\omega\gg 1}{\sim} \frac{1}{\mu/\omega}\,. \tag{2}$$

Its polynomial decay significantly improves the success of the spectral reconstruction already for Mastubara correlators with $\omega = \omega_n$. Such a rational kernel is moreover an analytic implementation of the idea behind the Backus-Gilbert [35] or Sumudu [36] approaches.

In summary, it is the combination of the rational kernel in (2) and the access to arbitrary frequencies that leads to exponentially improved accuracy in the spectral reconstruction, see Fig. 3 for the results.

Now we discuss the lattice setup that implements the above ideas. The starting point is a real-time thermal field theory, formulated on the Schwinger-Keldysh contour [37, 38]:

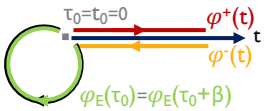

It amounts to an initial value problem with the following path integral representation for the partition function $\mathcal{Z}$,

$$\underbrace{\int [d\varphi_0^+][d\varphi_0^-]\langle\varphi_0^+|e^{-\beta\hat{H}}|\varphi_0^-\rangle}_{\text{initial conditions}} \underbrace{\int_{\varphi_0^+}^{\varphi_0^-} \mathcal{D}\varphi e^{iS_M[\varphi^+]-iS_M[\varphi^-]}}_{\text{quantum dynamics}}, \tag{3}$$

where $\hat{H}$ denotes the Hamiltonian and S_M the Minkowski space action. $\varphi^+(t,\mathbf{x})$ lives on the forward branch from $t_0 = 0$ to t, and $\varphi^-(t,\mathbf{x})$ lives on the backward branch. The initial conditions can be rewritten as a path integral for $\varphi_E(\bar{\tau},\mathbf{x})$ on a compact imaginary time axis $\bar{\tau} \in [0,\beta]$.

We now analytically continue the real-time contour to a Euclidean domain τ that differs from the compact imaginary time axis $\bar{\tau}$ used for the initial conditions. The forward branch $\varphi^+(\tau)$ may be discretized using stochastic quantization [39] with a Euclidean action S_E. The sign of S_E on the backward branch renders a similar treatment of $\varphi^-(\tau)$ non-convergent. This φ^--pathology propagates to φ^+ for any finite extent of the contour: forward and backward branch are connected via the boundary at the latest time $\tau_{\rm max}$ as derivatives in S_E couple neighboring sites. This is a finite lattice spacing artefact.

The above issue is resolved by dropping the $\varphi^+\varphi^-$-terms that are lattice artifacts. After decoupling φ^+ and φ^- it suffices to concentrate on the φ^+-contour. The imaginary frequency propagator in (2) is simply given by

$$G(\omega) = G^{++}(\omega) := \langle \varphi^+(\omega)\varphi^+(-\omega)\rangle\,, \qquad (4)$$

and $G^{++}(\omega) = -G^{--}(\omega)$. Similar identities hold for higher correlation functions. Technically, the φ^+-contour now has a boundary at $\tau_{\rm max}$. The behavior of $\varphi^+(\tau_{\rm max})$ should be fixed such that the continuum and infinite time limit is reached efficiently. We have failed to reach convergence with free boundary conditions. Setting the field to zero or periodically continuing it with $\varphi^+(\tau_0) = \varphi^+(\tau_{\rm max}) = \varphi_E(\bar{\tau}_0)$ leads to slow convergence. This can be attributed to the initial condition $\varphi^+(\tau_0) = \varphi_E(\bar{\tau}_0)$. Even in the free theory it imprints a temperature dependence on the $\varphi^+(\tau)$-correlators, that only disappears in the continuum limit.

This lattice artefact can be removed as follows: for periodic boundary conditions the Fourier transform to frequency space translates the initial condition to the constraint $\sum_l \varphi^+(\omega_l) = \varphi_E(\bar{\tau}_0)$, where $|l| = 0, ..., \lfloor N_\omega/2\rfloor$, and $\omega_l = 2\pi l/(N_\omega \Delta\bar{\tau})$. Here $\Delta\bar{\tau}$ is the temporal lattice spacing on the standard Euclidean lattice. This constraint can be rewritten as one for the field at the highest frequency, $\varphi^+(\omega_{\lfloor N_\omega/2\rfloor}) = \varphi_E(\bar{\tau}_0) - \sum_l \varphi^+(\omega_l)$. The kinetic term $1/2\sum_l \varphi^+(\omega_l)\mathcal{P}(\omega_l)\varphi^+(\omega_l)$ with lattice dispersion $\mathcal{P}$ is local in frequency space. Therefore, the constraint is irrelevant in the continuum limit, as its statistical weight is vanishing due to $\varphi^+(\omega_{\lfloor N_\omega/2\rfloor})\mathcal{P}(\omega_{\lfloor N_\omega/2\rfloor})\varphi^+(\omega_{\lfloor N_\omega/2\rfloor}) \to \infty$. Hence the constraint can be already dropped on the lattice for all terms local in frequency space, thereby improving the continuum limit. Here we apply this reasoning to S_0, the quadratic part of the action. The efficient convergence of this approach is confirmed for the propagator, see Fig. 2.

Then, the full theory is formulated in a mixed representation in τ and ω. While S_0 is simulated in ω-space, $S_{\rm int} = S - S_0$ is directly implemented in τ-space for local interactions on the sites. Hence, the thermal initial condition $\varphi^+(\tau_0) = \varphi_E(\bar{\tau}_0)$ solely enters via the interaction term. For derivative interactions we also drop the mixed $\varphi^+\varphi^-$-terms at the boundary in $S_{\rm int}$. This introduces a finite volume effect, which vanishes as $N_\omega \to \infty$.

This concludes the formulation and discussion of our lattice setup. Our novel approach is now tested in a $0+1$ dimensional scalar field theory at temperature $T = 1/\beta$, whose Euclidean action reads

$$S_E = \int d\tau \big(\underbrace{\frac{1}{2}(\partial_\tau \varphi_E)^2 + \frac{1}{2}m^2\varphi_E^2}_{S_E^0} + \underbrace{\frac{\lambda}{4!}\varphi_E^4}_{S_E^{\rm int}} \big)\,.$$

The system is simulated on a frequency lattice with N_ω points using stochastic quantization,

$$\partial_{t_5}\varphi^+(\omega_l) = -\frac{\delta S_0}{\delta\varphi^+(\omega_l)} - \frac{\delta S_E^{\rm int}}{\delta\varphi^+(\tau_j)}\frac{\delta\varphi^+(\tau_j)}{\delta\varphi^+(\omega_l)} + \eta(\omega_l)\,. \quad (5)$$

Here a sum over $j = 1, ..., N_\omega$ is implied and the dispersion reads $\mathcal{P}(\omega_l) = (2 - 2\cos[2\pi l/N_\omega])/\Delta\bar{\tau}^2$, $l \in [0, N_\omega - 1]$. In (5) $\eta(\omega_l)$ is the Fourier transform of the Gaußian noise, $\langle\tilde{\eta}(\tau_i)\tilde{\eta}(\tau_j)\rangle = 2\delta_{ij}/\Delta\bar{\tau}$ and S_0 represents the discretized free action,

$$S_0 = \sum_l \Delta\omega\, \frac{1}{2}\big(\mathcal{P}(\omega_l) + m^2\big)|\varphi^+(\omega_l)|^2\,, \qquad (6)$$

while $S_E^{\rm int} = S_E - S_0$ is the interaction term. Concurrently we sample the thermal initial conditions at N_τ points along the compactified Euclidean time τ,

$$\partial_{t_5}\varphi_E(\bar{\tau}_k) = \frac{-\delta S_E}{\delta\varphi_E(\bar{\tau}_k)} + \eta(\bar{\tau}_k),\ \langle\eta(\bar{\tau}_i), \eta(\bar{\tau}_j)\rangle = 2\frac{\delta_{ij}}{\Delta\bar{\tau}}\,. \quad (7)$$

so that the value of $\varphi^+(\tau = \tau_0)$ can be replaced with $\varphi_E(\bar{\tau} = \bar{\tau}_0)$ each time when computing $\frac{\delta S_E^{\rm int}}{\delta\varphi^+(\tau_j)}$ in (5). After $\Delta t_5 = 1$ we record the correlators $G_E(\bar{\tau}) = \langle\varphi_E(\bar{\tau})\varphi_E(0)\rangle$ and $G^{++}(\omega) = \langle\varphi^+(\omega)\varphi^+(-\omega)\rangle$, collecting in total $N_{\rm conf} = 10^6$ samples, which leads to a relative statistical error $\Delta G/G \sim 10^{-3}$.

To crosscheck our computations we have also performed an equivalent quantum mechanical (QM) computation of the thermal real-time correlation functions $G^{\rm QM}(t) \equiv \langle\hat{x}(t)\hat{x}(0)\rangle$ using the anharmonic oscillator in the truncated Hilbert space of 32 energy eigenfunctions of the harmonic oscillator [37]. The spectral function is obtained from a Fourier transform of $\mathrm{Im}[\langle\hat{x}(t)\hat{x}(0)\rangle]$ along $N_t = 3.2 \times 10^4$ steps of $\Delta t = 0.05$, i.e. it is computed only over a finite real-time extent. Due to the restricted Hilbert space and integration this computation underestimates the height of delta-peak like structures, present e.g. in the free spectrum and contains ringing.

In Fig.1 we show the Euclidean correlators computed for the thermal scalar system at $\beta = 1$ and $m = 1$ along the standard compactified Euclidean axis for the free $\lambda = 0$ case (top points) and the interacting case $\lambda = 24$ (bottom points). The black crosses denote the outcome of the quantum mechanical computation and open symbols denote lattice results. For the free case we only carry out simulations at $N_{\bar{\tau}} = 16$, while at $\lambda = 24$

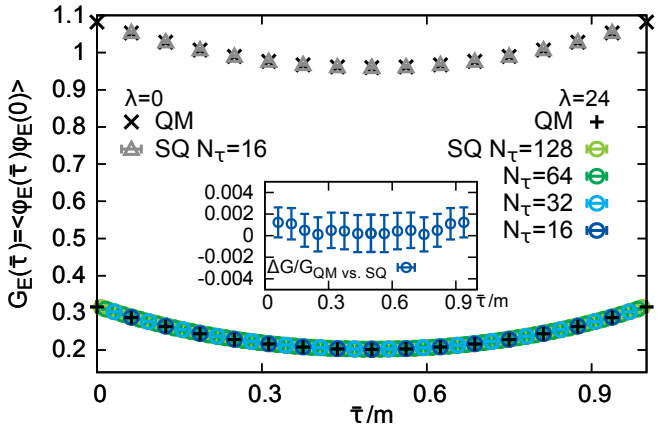

FIG. 1. Euclidean correlation functions $G_E(\bar{\tau})$ for $\lambda = 0$ (upper points) and $\lambda = 24$ (lower points). Black crosses denote correlators from a quantum mechanical computation, while open symbols represent standard lattice simulations. The inset shows the relative difference between the lattice result for $\lambda = 24$ at $N_{\bar{\tau}} = 16$ and the quantum mechanical computation.

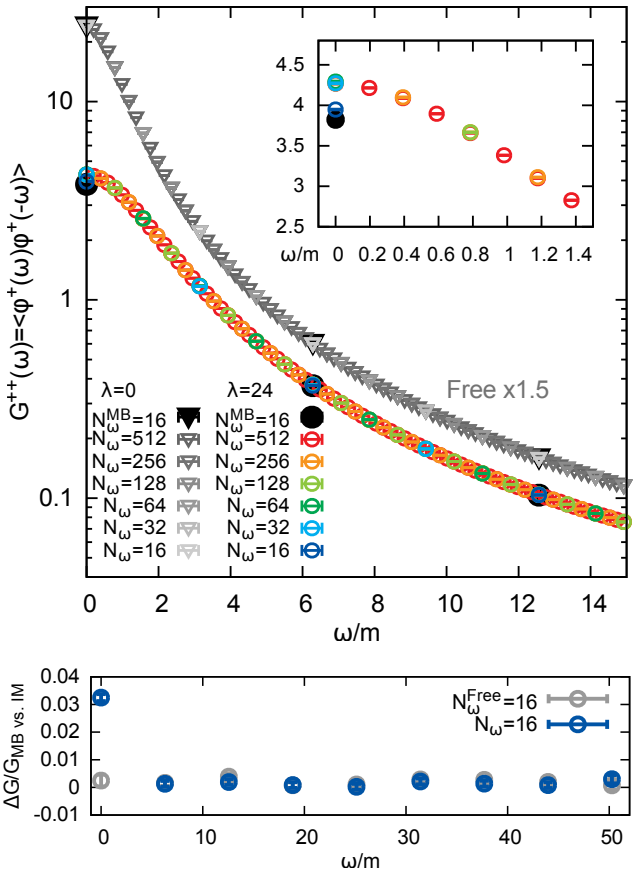

FIG. 2. (top) Imaginary frequency correlators $G^{++}(\omega)$ from lattice simulations at $\lambda = 0$ (gray, shifted $\times 1.5$) and at $\lambda = 24$ (colored). Black filled symbols correspond to the correlator at the Matsubara frequencies accessible in standard simulations. Open symbols arise from our imaginary frequency simulation. The inset shows the low frequency regime at $\lambda = 24$, in particular that finite volume artifacts are present at ω_0 in the Matsubara correlator, which are removed going to finer resolution in ω. (bottom) Relative difference standard Matsubara correlators and those from our direct simulation. Note the excellent agreement except for ω_0 at $\lambda = 24$, reflecting finite volume artifacts in the standard Matsubara value.

we produce data at four different $N_{\bar{\tau}} = 16 \ldots 128$. The inset shows the relative difference between the interacting correlator at $N_{\bar{\tau}} = 16$ computed from the lattice and via quantum mechanics. For our choice of $dt_5 = 10^{-4}$ they agree within the statistical errors of the lattice simulation. Note that if $N_{\bar{\tau}}$ is increased, it corresponds to a higher resolution of the $\bar{\tau}$ interval which leads to a larger drift term, so that to have an accurate outcome at $N_{\bar{\tau}} = 128$ the Monte Carlo time step already needs to be reduced by two orders of magnitude.

We focus on simulations with $N_{\bar{\tau}} = 16$, and inspect the corresponding correlation functions in imaginary frequency space given in the top panel of Fig.2 for both the free (gray) and interacting (colored) case. We show only the relevant low frequency regime up to $\omega/m = 15$ while the simulations reach up to $\omega_8/m \approx 50$. As $\varphi^+(\tau) \in \mathbb{R}$ the correlators are real and symmetric around $\omega = 0$.

The black filled symbols denote the correlators obtained from simply Fourier transforming the fields along the compact Euclidean domain and thus are located at the Matsubara frequencies ω_n. The open symbols are obtained from the fields simulated directly along the imaginary frequency domain using between $N_\omega = 16 \ldots 512$ points. In the free $\lambda = 0$ case our novel simulation yields a smooth interpolation between the Matsubara frequencies and furthermore as can be seen from the gray points in the lower panel of Fig.2 agrees excellently with the values obtained from the Fourier transform of the compact Euclidean domain. Note that at $\lambda = 0$ the two concurrent simulations (5) and (7) are completely decoupled.

In the interacting case denoted by colored open symbols in Fig.2, we again find a smooth interpolation between Matsubara frequencies and very good agreement with the standard Matsubara propagators for $\omega_{n>0}$. Let us inspect the regime close to the origin, given by the inset on the top of Fig.2. Already at $N_\omega = 16$ the new simulation (dark blue) leads to a value at $\omega = 0$ that differs from the conventional Matsubara one (black). Increasing N_ω quickly lets the correlator converge significantly above the standard estimate. Since in a lattice simulation $\omega = 0$ reflects the sum over all corresponding imaginary time extent, we infer that the standard simulation along the compactified Euclidean domain is not able to capture all the relevant late Euclidean-time physics that however can be vital to thermal processes. Its purpose is only to correctly sample $\varphi(\bar{\tau}_0)$, which it does.

Now we extract spectral functions from the data, with kernels $\tilde{K}(\mu, \bar{\tau}, T) = \cosh[\mu(\bar{\tau} - /2T)]/\sinh[\mu/2T]$ and

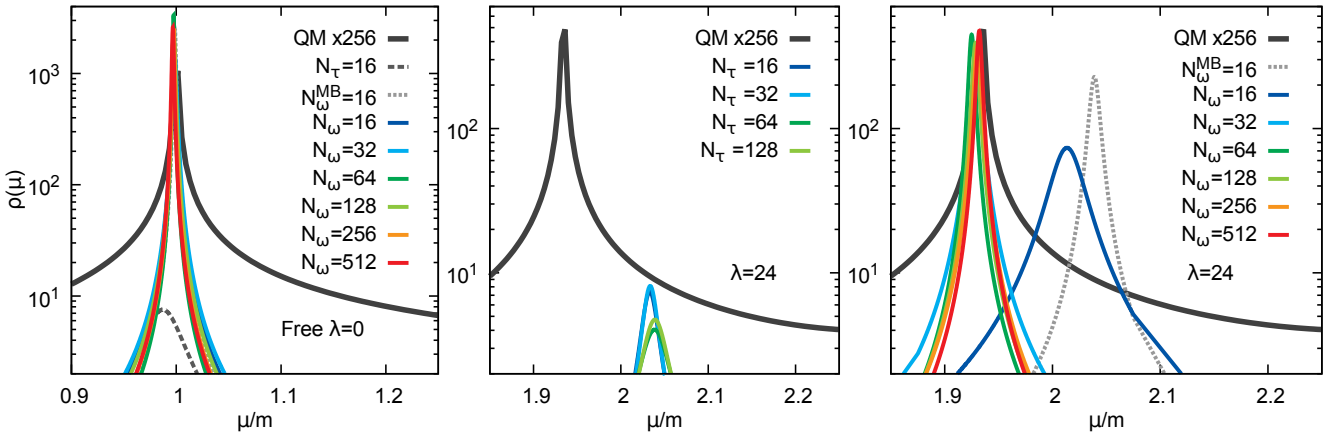

FIG. 3. Spectral functions of the free theory (left) and at $\lambda = 24$ unfolded from Euclidean (center) and imaginary frequency correlators (right). In each panel $\rho(\mu)$ from the corresponding quantum mechanical computation is plotted as solid thick gray line. Spectra denoted by N_τ are reconstructed from Euclidean correlators and $N_\omega^{\rm MB}$ from the Fourier transformed Matsubara one. The label N_ω refers to spectra from the direct imaginary frequency simulation resolving between ω_n.

$K(\mu,\omega) = \frac{2\mu}{\mu^2+\mathcal{P}(\omega)}$. The latter is the lattice analogue of the continuum Källén-Lehmann kernel, and its use leads to a more efficient convergence of the spectral reconstruction. Here we deploy a recent Bayesian reconstruction (BR) method [40] and discretize positive real-time frequencies $\mu \in [10^{-3}, 200]$ with $N_\mu = 4000$ points including a high frequency window of $N_\mu^{\rm HP} = 1000$ around the lowest lying peaks. For minimal bias we use a flat default model $m(\mu) = 1$. In the free case we know that only a single delta-peak at the mass of the field exists in the spectrum. The quantum mechanical computation given by the thick gray line in the left panel of Fig.3 while being able to capture the position of the peak, gives an artificial finite width due to the underlying finite real-time extent Fourier transform. We have checked that it can be reduced systematically and therefore for visualization purposes multiply the curve here by a factor of 256. The reconstruction from the $N_{\bar\tau} = 16$ compact Euclidean domain (dark gray dashed) both gives a too large width and its position is still slightly off. A Fourier transform of the Euclidean fields and reconstructing along Matsubara frequencies already improves the results significantly. The light gray dashed line shows a much reduced width and is positioned very close to unity. Since here the standard Matsubara data already leads to a very good result, the improvement from using the correlators of the new simulation only leads to a further decrease in the reconstructed width. Note that the width depends on the error of the data and can be improved by more statistics.

Turning to the interacting case $\lambda = 24$, we first carry out the reconstruction from Eucldiean data, using different resolutions along $\bar\tau$. In the center panel of Fig.3 the results are shown for $N_{\bar\tau} = 16 \ldots 128$. We find that the reconstruction does not capture the position of the lowest lying peak in the spectrum and even more importantly does not show a systematic improvement with $N_{\bar\tau}$. The reason is that with larger $N_{\bar\tau}$ higher ω_n become accessible but contribute only marginally to the relevant physics.

If on the other hand we use data in imaginary frequency space the situation is very different as shown in the right panel of Fig.3. Again simply using the standard Matsubara correlators already improves the width of the reconstruction while the peak position is still off (gray dashed). However the access to the correlator at frequencies between ω_0 and ω_1 allows us to systematically and significantly improve the reconstruction of the lowest lying peak, with $N_\omega = 512$ reproducing the peak position with high accuracy.

In summary we have shown that by carefully distinguishing initial conditions from quantum dynamics it is possible to devise a simulation prescription for thermal quantum fields along general imaginary frequencies. In particular this approach gives access to the thermal physics between ω_0 and ω_1. Real-time spectral functions are related to imaginary time correlators via an integral transform with a rational kernel, and in combination their extraction becomes exponentially improved. The success of this approach has been demonstrated here with scalar fields. It can be straightforwardly extended to Abelian and non-Abelian gauge theories which is work in progress. Evidently, computations of phenomenologically relevant quantities such as transport coefficients and heavy quark spectral functions will be improved significantly with our simulation prescription.

We thank N. Christiansen for discussions. A.R. acknowledges fruitful exchanges at the ECT* workshop on advances in transport. This work is supported by EMMI, the grants ERC-AdG-290623, BMBF 05P12VHCTG. It is part of and supported by the DFG Collaborative Research Centre "SFB 1225 (ISOQUANT)".

[1] B. Mueller, Phys. Scripta **T158**, 014004 (2013), 1309.7616.
[2] N. Armesto and E. Scomparin, European Physical Journal Plus **131**, 52 (2016), 1511.02151.
[3] I. Bloch, J. Dalibard, and W. Zwerger, Rev. Mod. Phys. **80**, 885 (2008).
[4] A. Adams, L. D. Carr, T. Schäfer, P. Steinberg, and J. E. Thomas, New Journal of Physics **14**, 115009 (2012), 1205.5180.
[5] U. Heinz, C. Shen, and H. Song, AIP Conf. Proc. **1441**, 766 (2012), 1108.5323.
[6] S. Ryu *et al.*, Phys. Rev. Lett. **115**, 132301 (2015), 1502.01675.
[7] H. B. Meyer, Phys. Rev. Lett. **100**, 162001 (2008), 0710.3717.
[8] K. Kamikado, N. Strodthoff, L. von Smekal, and J. Wambach, Eur. Phys. J. **C74**, 2806 (2014), 1302.6199.
[9] M. Haas, L. Fister, and J. M. Pawlowski, Phys.Rev. **D90**, 091501 (2014), 1308.4960.
[10] N. Christiansen, M. Haas, J. M. Pawlowski, and N. Strodthoff, Phys. Rev. Lett. **115**, 112002 (2015), 1411.7986.
[11] G. Aarts *et al.*, JHEP **02**, 186 (2015), 1412.6411.
[12] S. W. Mages, S. Borsnyi, Z. Fodor, A. Schaefer, and K. Szab, PoS **LATTICE2014**, 232 (2015).
[13] H.-T. Ding, O. Kaczmarek, and F. Meyer, Phys. Rev. **D94**, 034504 (2016), 1604.06712.
[14] C.-C. Chien, S. Peotta, and M. Di Ventra, Nat Phys **11**, 998 (2015).
[15] C. Cao *et al.*, Science **331**, 58 (2011), 1007.2625.
[16] T. Enss, R. Haussmann, and W. Zwerger, Annals Phys. **326**, 770 (2011), 1008.0007.
[17] H. T. Ding *et al.*, Phys. Rev. **D86**, 014509 (2012), 1204.4945.
[18] G. Aarts *et al.*, JHEP **07**, 097 (2014), 1402.6210.
[19] S. Kim, P. Petreczky, and A. Rothkopf, Phys. Rev. **D91**, 054511 (2015), 1409.3630.
[20] S. Borsanyi *et al.*, JHEP **04**, 132 (2014), 1401.5940.
[21] Y. Burnier, O. Kaczmarek, and A. Rothkopf, JHEP **12**, 101 (2015), 1509.07366.
[22] E. Wille *et al.*, Phys. Rev. Lett. **100**, 053201 (2008).
[23] Y. Nishida, Phys. Rev. **A79**, 013629 (2009), 0811.1615.
[24] W. M. C. Foulkes, L. Mitas, R. J. Needs, and G. Rajagopal, Rev. Mod. Phys. **73**, 33 (2001).
[25] J. Smit, Cambridge Lect. Notes Phys. **15**, 1 (2002).
[26] G. Aarts and J. Berges, Phys. Rev. **D64**, 105010 (2001), hep-ph/0103049.
[27] S. Strauss, C. S. Fischer, and C. Kellermann, Phys.Rev.Lett. **109**, 252001 (2012), 1208.6239.
[28] R.-A. Tripolt, N. Strodthoff, L. von Smekal, and J. Wambach, Phys.Rev. **D89**, 034010 (2014), 1311.0630.
[29] A. J. Helmboldt, J. M. Pawlowski, and N. Strodthoff, Phys.Rev. **D91**, 054010 (2015), 1409.8414.
[30] J. M. Pawlowski and N. Strodthoff, Phys. Rev. **D92**, 094009 (2015), 1508.01160.
[31] T. Yokota, T. Kunihiro, and K. Morita, PTEP **2016**, 073D01 (2016), 1603.02147.
[32] K. Kamikado, T. Kanazawa, and S. Uchino, (2016), 1606.03721.
[33] C. Jung, F. Rennecke, R.-A. Tripolt, L. von Smekal, and J. Wambach, (2016), 1610.08754.
[34] M. Jarrell and J. Gubernatis, Physics Reports **269**, 133 (1996).
[35] B. B. Brandt, A. Francis, H. B. Meyer, and D. Robaina, Phys. Rev. **D92**, 094510 (2015), 1506.05732.
[36] F. Pederiva, A. Roggero, and G. Orlandini, J. Phys. Conf. Ser. **527**, 012011 (2014).
[37] J. Berges, S. Borsanyi, D. Sexty, and I. O. Stamatescu, Phys. Rev. **D75**, 045007 (2007), hep-lat/0609058.
[38] J. Berges, (2015), 1503.02907.
[39] M. Namiki *et al.*, Lect. Notes Phys. **M9**, 1 (1992).
[40] Y. Burnier and A. Rothkopf, Phys. Rev. Lett. **111**, 182003 (2013), 1307.6106.